Solar Energy Materials & Solar Cells 269 (2024) 112799

Contents lists available at ScienceDirect

Solar Energy Materials and Solar Cells

journal homepage: www.elsevier.com/locate/solmat

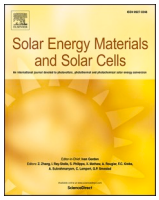

Enhancing dielectric-silicon interfaces through surface electric fields during firing

Ruy S. Bonilla [a,*], Isabel Al-Dhahir [a], Xinya Niu [a], Pietro P. Altermatt [b], Phillip Hamer [c]

[a] Department of Materials, University of Oxford, Oxford, OX1 3PH, United Kingdom
[b] Trina Solar, State Key Laboratory for Photovoltaic Science and Technology (SKL PVST), Xinbei District, Changzhou, Jiangsu Province, 213031, China
[c] School of Photovoltaic and Renewable Energy Engineering, The University of New South Wales, Kensington, NSW, 2052, Australia

ARTICLE INFO

Keywords:
Silicon photovoltaics
Surface passivation
Dielectric thin films
Corona electric field
Carrier recombination

ABSTRACT

Minimising charge losses at silicon interfaces is a major development area for highly efficient solar cells. Here we report on the interface improvements achieved by establishing a surface electric field during low-temperature firing of dielectric thin films. By inducing a corona electric field on the surface of a thin film stack, we observe significant modifications to the silicon-dielectric interface upon annealing, which correlate with the characteristics of interface defects. The passivation properties of the interfaces strongly depend on the polarity and strength of the electric field during firing, as well as the dielectric materials in the layer stack. We show that the surface electric fields not only influence surface carrier population but also affect the resulting chemical interface properties post-annealing. It is postulated that hydrogen migration plays a role in these observed effects. Leveraging the corona-induced electric field enables fine-tuning of both the chemical and field-effect passivation in thin film surface dielectrics, resulting in recombination current densities as low as 2.8 fA cm^{-2} in research-grade float zone silicon, and 14 fA cm^{-2} in industrial-grade textured silicon. The simplicity and versatility of the thin film electric polarisation enable a new strategy for controlling and exploiting the chemical enhancement of interfaces in solar cell devices, from current TOPCon and PERC devices to future multijunction silicon-based cells.

1. Introduction

Silicon solar cells have been extremely successful due to their high performance, low cost, and long stability [1–3]. Efficient cells, however, require stable and effective methods to avoid the recombination of photo-generated carriers, commonly termed passivation [4]. Surface recombination is particularly detrimental to the performance of the cell. Due to the crystal periodicity's termination, many defects are normally located at the surface [5]. There are two methods to minimise surface carrier recombination. The first is to reduce the concentration of defects through chemical passivation, where a dielectric layer is deposited onto the surface to bind to the non-coordinated silicon bonds [5]. This eliminates the recombinative trap sites produced by such dangling bonds. This method can be further improved via thermal processing of such dielectric layers, to induce hydrogen migration towards the silicon-dielectric interface [6]. This process allows H to passivate any remaining Si dangling bonds. The second method is to use field effect passivation (FEP) to control the surface carrier concentration and limit the access of minority carriers to defect sites. FEP uses an electric field to control the population of charge carriers present at the interface, creating a space-charge region [7]. The electric field can be produced through the native charge that exists in dielectric layers [8]. However, the field can be further and more precisely manipulated either through the deposition of corona charges [9] or by incorporating stable fixed charges at the interface, such as potassium ions [10,11].

Hydrogen passivation is a well-demonstrated phenomenon [12–14]. Presently, hydrogenated dielectrics are ubiquitous in industrially manufactured solar cells [12,15,16]. Typical dielectrics used in commercial cells are hydrogenated amorphous silicon (a-Si:H), hydrogenated silicon nitride (SiN_x:H) and aluminium oxide (AlO_x), all typically grown via plasma enhanced chemical vapour deposition (PECVD). Atomic hydrogen is introduced to the dielectric during PECVD using hydrogen-containing precursor gases such as ammonia, silane, or trimethylamine [17–19]. Once in the dielectric, hydrogen can exist in three charged states: positive (H^+), negative (H^-) and neutral (H^0) [20,21]. The predominance of one charge state over the other depends upon

* Corresponding author.
E-mail address: sebastian.bonilla@materials.ox.ac.uk (R.S. Bonilla).

https://doi.org/10.1016/j.solmat.2024.112799
Received 27 January 2024; Received in revised form 20 February 2024; Accepted 1 March 2024
Available online 10 March 2024

the position of the Fermi level relative to the acceptor and donor levels of atomic hydrogen within the insulator or semiconductor [22]. It has been reported that H^+ is the most stable charge state of hydrogen at the Si-SiO_x interface [23,24]. In view of the existence of charged hydrogen, here we hypothesise that it should be possible to control H^+ migration across a dielectric thin film by using an electric field [25]. Furthermore, the polarity of molecules in recently reported liquid passivation schemes may also be controlled by an electric field [26–28], thus changing the interface mechanisms. It is rather complex to unambiguously ascribe changes in surface passivation to the presence of H. This is especially cumbersome as the interfacial concentrations are much smaller than typical mass spectroscopy detection limits, and can have a strong optoelectronic influence. We hence decided to use optoelectronic characterisation to identify the interface chemical passivation that arises from such hypothesised H migration behaviour.

We investigate the impact that surface charge on SiN_x has on the chemical passivation performance at the SiO_2–Si interface. The interface passivation is evaluated via effective lifetime and capacitance-voltage measurements, and is found to be heavily influenced by the polarity and magnitude of the electric field. Under optimal interface chemical and charge-assisted passivation, a maximum lifetime of 6 ms is achieved in n-type 1 Ω cm float zone silicon, equivalent to a surface recombination velocity (SRV) < 1 cm/s and current density $J_{0s} < 2.8$ fA cm^{-2}. In contrast, when a surface electric field is set to non-optimal (presumed removal of interfacial hydrogen) conditions, the dielectric-Si interface worsens, and the lifetime reduces to ~300 μs, with SRV increasing to values as high as ~140 cm/s. We therefore find that the electric field condition of the dielectric thin films is crucial to fully exploit the maximum surface passivation performance.

2. Sample preparation and methodology

In this work we use three starting substrates. Substrate A was a 200 μm thick, n-type 1 Ω cm Float Zone (FZ) 4-inch silicon wafer. Substrate B is textured FZ with the same conditions as A, except that B underwent texturing to form random pyramids before oxidation textured using a standard wet chemical KOH/IPA etch [29]. These were tested to investigate a commercially relevant surface finish and oxidation step. Sample Set C consisted of industrially sourced Czochralski M2 silicon wafers (156 mm pseudo squares), 135 μm thick, 5–10 Ω cm, textured and processed in high throughput industrial facilities, including oxidation furnaces or batch tube-based PECVD reactors.

In substrate A, a 100 nm thermal SiO_2 was grown at 1050 °C in oxygen and dichloroethylene at Fraunhofer ISE, followed by a forming gas anneal in a tube furnace at 425 °C for 30 min. Set A.1 were SiO_2 control samples with no further treatment [29].Set B.1 had a 10 nm thermally grown SiO_2, at 950 °C, before a forming gas anneal at 425 °C was carried out, identical to that applied to planar specimens A. Following this, wafers were cleaved into quarters, and four types of samples were created and tested. Sets A and B were all ¼ of a 4-inch wafer, with approximately 5 cm flat-edge length. Set C.1 had oxidation carried out at 900 °C to produce a ~5 nm SiO_2 nanolayer. Full wafers were used for subsequent testing.

On sets A.2-4 and B.2-4, a single layer of ~64 nm SiN_x was deposited on top of the oxide layer via PECVD (Oxford Instrument PlasmaLab 80+) with silane and ammonia as precursor gases. The deposited SiN_x had a refractive index of n = 1.9 as measured using four-wavelength ellipsometry on an FS1 Film Sense kit. In Subset C.2, PECVD of silicon nitride was carried out at 450 °C to produce a 60 nm layer with a refractive index of either 1.95, 2.1, or 2.4. The parameters for SiN_x deposition at industrial facilities are not disclosed.

Set X.2 were SiN_x control samples, with no further treatment. Sets X.3 and X.4 had positive and negative corona charge deposited, respectively, on both sides of the wafer from a steel point electrode held 20 cm above the wafer at ±30 kV. This was immediately followed by annealing at 450 °C in air, for 20 s, unless otherwise stated. This process was termed a corona-anneal (C-A).

The effective lifetimes of all sample sets were recorded using a Sinton WCT-120 Lifetime Tester (ver 4.6.0). The transient method, with a 1/64 s light pulse was used on all samples except where lifetimes remained below 200 μs? For such low lifetimes, the quasi-steady state method (1/1 s light pulse) was used. All lifetime values are quoted at an injection level of 10^{15} cm^{-3}. To estimate the fundamental interface recombination parameters, surface recombination at the oxide-silicon interface was varied by regulating the surface carrier population using a biased transparent gate. The recently established method in Ref. [30] was used to record effective lifetime as a function of gate bias.

In this procedure, a semi-transparent gate electrode is produced on top of the dielectric to simultaneously control surface potential and measure effective lifetime on the Sinton Lifetime Tester. Undiluted poly (3,4-ethylenedioxythiophene)-poly(styrenesulfonate) (PEDOT:PSS) was coated over both sides of all finished samples with a standard paintbrush to form a nearly transparent thin film. After coating, the film was annealed at ~120 °C in air, for 2 min to increase the conductivity [31,32]. The PEDOT:PSS solution was 3.0–4.0 wt % in H_2O from Sigma Aldrich. An analytical model was used to fit the experimental lifetime versus surface charge data and to quantify the interface recombination parameters. The model was adapted from Girisch and Aberle's iterative formalism to calculate the density of carriers at the surface, with an extension to account for surface charge fluctuations [33–35]. Further details on the model are described in the Supplementary Materials. A schematic diagram of all processing in this work is shown in Fig. 1.

To find the effective surface recombination parameters S_{eff} and J_{0s}, the surface effective lifetime, τ_s, was calculated assuming a bulk Shockley-Read-Hall (SRH) lifetime, τ_{SRH} [36]. This followed the iterative algorithm proposed by Kimmerle et al. [37] based on previous work by Mäckel and Verner [38] and by Kane and Swanson [39]. Values obtained via Kimmerle's algorithm are quoted here. The procedure goes as follows. Surface lifetime (τ_s) is given as:

$$\frac{1}{\tau_s} = \frac{1}{\tau_{eff}} - \frac{1}{\tau_{Rad}} - \frac{1}{\tau_{Aug}} - \frac{1}{\tau_{SRH}}. \tag{1}$$

First, τ_{SRH} is assumed infinite and a carrier dependent J_0 is calculated from a Sinton photoconductance measurement as:

$$J_0(\Delta n) = \frac{d}{d\Delta n}\left(n_{i,eff}^2 \cdot \sqrt{D\left(\frac{1}{\tau_s}\right)} \tan\left(\frac{W}{2}\sqrt{\frac{1}{D}\left(\frac{1}{\tau_s}\right)}\right)\right), \tag{2}$$

where Auger and radiative recombination are described by Niewelt's parameterisation [40], and the effective intrinsic concentration $n_{i,eff}(\Delta n)$ is calculated using PV Lighthouse's [41] implementation of Pässler's model [42]. The surface saturation current density, J_{0s}, is then calculated as the average around the ± 10 % of the flattest part of the $J_0(\Delta n)$ curve. The flattest part was defined by the minimum of $dJ_0(\Delta n)/d\Delta n$.

After finding an injection-independent J_{0s}, the SRH term that best satisfies

$$\frac{J_{0s} * (N_{dop} + \Delta n)}{q n_{i,eff}^2} = \sqrt{D\left(\frac{1}{\tau_s}\right)} \tan\left(\frac{W}{2}\sqrt{\frac{1}{D}\left(\frac{1}{\tau_s}\right)}\right), \tag{3}$$

is found numerically using a Nonlinear Least Squares minimisation in Matlab. Once a $\tau_{SRH}(\Delta n)$ is found, an average injection independent τ_{SRH} is found averaging the same range of Δn as previously done for $J_0(\Delta n)$. This procedure is iterated until τ_{SRH} and J_{0s} change marginally. The resultant value of τ_{SRH} is then used in τ_s to find S_{eff}. Thorough explanation of these algorithms can be found in the work of Hammann [43]. For completeness, the best fit of the experimental τ_{eff} obtained via the above algorithm is included.

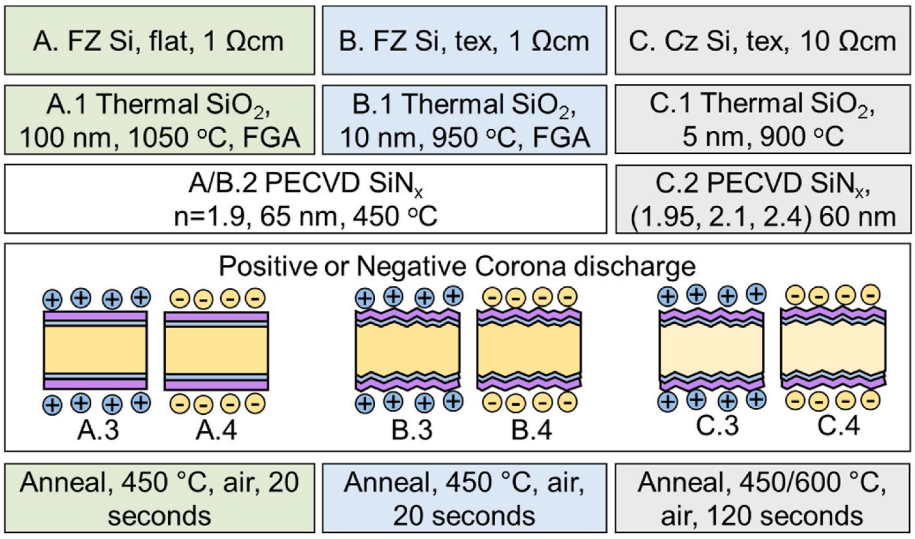

Fig. 1. Schematic diagram of the process flow for all samples reported in this work.

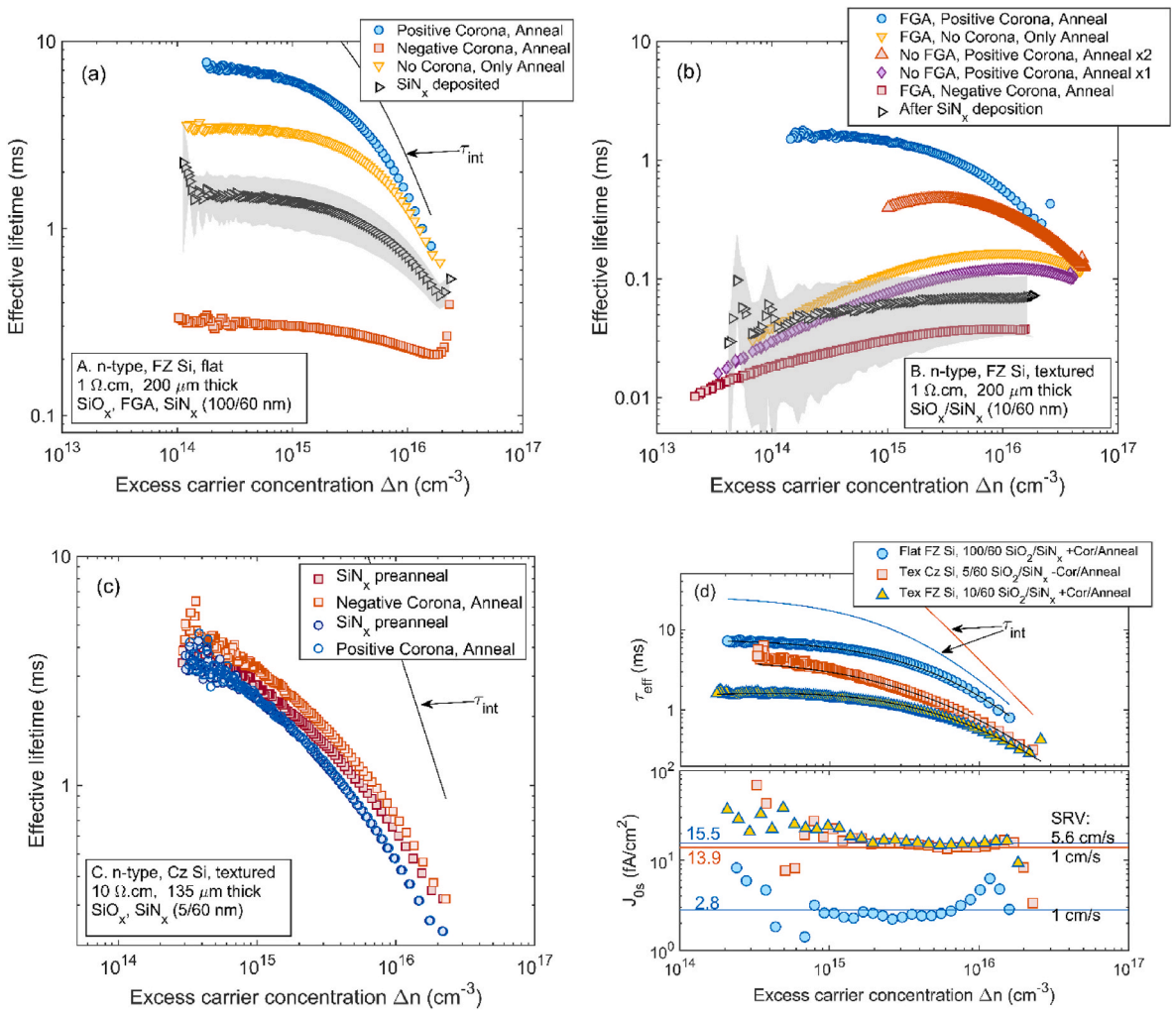

Fig. 2. Effective lifetimes before and after polarised anneal, including positive and negative surface electric fields. (a) For n-type FZ Si flat specimens passivated with 100/60 nm of SiO_2-SiN_x thin film stacks. (b) For n-type FZ Si textured specimens passivated with 10/60 nm of SiO_2-SiN_x thin film stacks. (c) For industrial n-type Cz Si textured specimens passivated with 5/60 nm of SiO_2-SiN_x thin film stacks. (d) Extraction of surface recombination parameters J_{0s} and SRV (bottom), from fitting of τ_{eff} (top). Best fit shown by black solid lines. Intrinsic lifetime limits are included in solid lines, blue (sample A) and red (sample B).

3. Effect of surface electric fields during anneals

We start by testing our previous findings where surface electric fields can impact the chemical passivation of SiO_2-SiN_x double-layer stacks [44]. The effective lifetime of symmetrically passivated SiO_2-SiN_x samples, pre and post-corona anneal, is illustrated in Fig. 2. The grey shaded area indicates the range of lifetimes obtained after SiN_x deposition. In Fig. 2a and b, we test high-quality FZ Si in groups A and B. One corona-anneal process was applied, with the corona discharge lasting 30 s, prior to a 450 °C anneal. As seen in Fig. 2 a, samples treated with positive charge recorded improvements in lifetime, while the sample treated with negative corona anneal decreased in final lifetime, when compared to the as-deposited SiN_x sample. The 30 s anneal was chosen to be sufficiently lengthy and dissipate the effects of corona-induced field effect passivation [45,46], as monitored by Kelvin Probe surface potential measurements. This means, the passivation obtained after annealing only originated from the obtained chemical passivation and the charge stored *inside* the SiO_2-SiN_x film stack. When samples are annealed without an added surface electric field, improvements in lifetime are also observed, presumably as the SiO_2-SiN_x stack already contains a concentration of positive charge.

To investigate the effectiveness of this technique in solar-relevant surfaces, textured wafers were similarly treated and tested using the optimal conditions found for positive corona charge. Textured wafers having only a thin oxide are of particular interest as they are commonly employed in industrial manufacture. Whilst these wafers benefit from increased light trapping due to the pyramidal arrangement [47,48], they experience greater recombination due to the increased surface area [47]. Additionally, the triangular pyramidal facets lie on the (111) planes, which possess a greater density of dangling bonds than the (100) plane of flat silicon [49]. Fig. 2 b illustrates lifetimes recorded for textured specimens in group B. It was found that the highest effective lifetime after a single positive corona-anneal was 1.4 ms at $\Delta n = 10^{15}$ cm^{-3}. This was achieved after 30 s of positive corona charge followed by a 20 s anneal at 450 °C. Here we have also tested FZ Si specimens without a forming gas anneal after oxidation. In such specimens the improvement after a single corona-anneal was only moderate, pointing to the importance of the presence of H during the anneal. We repeated the positive corona-anneal procedure twice, and we observed that the additional process produced substantial improvements in lifetime (orange upward triangles). Similar to group A, samples with negative surface potential degraded in lifetime, while samples without extrinsic positive fields showed only minor improvements (orange downward triangles).

Our previous work showed that there exists an optimal surface electric field strength before annealing [44]. Increasing the corona concentration beyond a saturation point worsens the lifetime. Hence, 30 s of corona discharge were found to work best for samples in groups A and B, which was equivalent to a total surface charge concentration of $+1.64 \times 10^{12}$ or -1.96×10^{12} q cm^{-2} for positive/negative corona (calibration included in the Supplementary Materials). One possible mechanism behind the deterioration of the passivation for excessively high positive surface electric fields is hot electron injection from the silicon to the oxide, as reported in Refs. [50,51]. Interface trap creation is reported to occur when electrons with energy ≥2 eV liberate hydrogen from defect sites [50,51]. However, Raskheev et al. asserted that only after hydrogen has been released from a defect site is it energetically favourable for the charged defect to capture a hot electron [24]. Another possible mechanism relates to the excessive concentration of H-forming defects, as reported in recent literature [52–54], and also observed by the authors. Section 5 will discuss the possible mechanisms involved, while an in-depth investigation into the relation to H kinetics will be addressed in future work.

The results in Fig. 2a and b show that a potential improvement in surface passivation can originate from the different polarity of the electric field prior to the anneal. Since surface passivation can be both chemical and field effect in origin, these results could imply that hydrogen, which exists in the dielectric in H^+ form, is migrating and chemically passivating the interface. When a positive electric field from the corona charge is present, it can promote hydrogen migration through the SiN_x dielectric to the Si–SiO_2 interface. At 450 °C, the hydrogen can diffuse rapidly through SiO_2 as reported in Refs. [55,56]. This suggests a 20-s anneal should be enough to reach the interface. Once at the interface, the hydrogen can passivate defect sites, raising effective lifetime to values as high as 6.2 ms at $\Delta n = 10^{15}$ cm^{-3}, in flat FZ Si. In contrast, the presence of a negative electric field results in low lifetimes of ~300 μs, which could be attributed to the inhibition of hydrogen migration through the dielectric, as well as the expulsion of hydrogen already located at interface states. It is noted here that due to the difficulties associated with measuring H, the above mechanisms are hypothesised rather than unambiguously ascribed to H migration.

We then extended the findings to industrial-grade material processed in high-throughput equipment (group C). Fig. 2 c illustrates the recorded effective lifetimes after positive and negative corona-anneal processes were applied to oxide-nitride passivated M2 wafers. Contrary to previous findings, a positive surface electric field did not improve the overall lifetime after annealing at 450 °C for 120 s. The longer anneal was chosen since the industrial SiN_x retained the surface corona charge for longer periods. When a negative surface charge was present, a moderate improvement in effective lifetime was observed (orange triangles in Fig. 2c). This indicated the inverse process than that proposed for samples in groups A and B. Further investigation was then required to assess the differences found. Additionally, it is known that corona charge during the anneals can embed some additional charge concentration into the film stack, which controls the surface charge carrier populations (n_s and p_s) via field effect. For positive (negative) charge, this would lead to lower (higher) recombination at the n-type surface. To distinguish the chemical and the field effect passivation, a further experiment was conducted, as will be described in Section 4. It revealed that both chemical and field-effect passivation are jointly increasing or reducing the passivation quality.

Prior to delving into the interface changes during corona anneals, we calculate the effective surface recombination parameters and illustrate them in Fig. 2 d. Here, the comparative surface recombination parameters for the highest-performing planar and textured samples are shown. Fig. 2 d top shows the injection level-dependent lifetimes of each sample, including the best-fitted model as per Kimmerle's formalism [37]. The highest lifetime achieved in this work for a planar wafer is 6.4 ms at $\Delta n = 10^{15}$ cm^{-3} for a SiO_2-SiN_x double layer, followed by corona charging for 30 s at + 30 kV and annealing at 450 °C for 20 s. This is equivalent to an SRV <1 cm/s and a J_{0s}, of 2.8 fA cm^{-2}, shown in Fig. 2 d bottom. This is in good agreement with values in the literature where corona-charged SiO_2-SiN_x dielectrics on 1 Ω cm Si have produced SRV ~0.15 cm/s [57]. The highest overall lifetimes for symmetrically processed textured FZ and Cz wafers are 1.4 ms and 3 ms, equivalent to an SRV< 5.6 and 1 cm/s at $\Delta n = 10^{15}$ cm^{-3}, respectively. Textured surfaces are prone to a higher concentration of surface defects and as a result, the recombination can be more than one order of magnitude higher than that of planar surfaces [58]. This gives rise to an increase in both the surface saturation current and surface recombination velocity of textured wafers. The recombination parameters calculated here have not been corrected for the increase in surface area occurring on a pyramidal textured surface. Baker-Finch and McIntosh [59] reported this increase to be $\times \sqrt{3}$. When corrected for the larger surface area, the best performing textured specimen in this work has SRV<0.5 cm/s, and a J_{0s} < 8 fA cm^{-2}. These are similarly low to those reported by Kho et al., where SRV and J_{0s} values of <1 cm/s and ~5 fA cm^{-2} were found, yet they required corona charged oxide-nitride-oxide stacks with an additional 450 °C, 30 min FGA [60].

4. Understanding changes in interface electrical characteristics

4.1. Research-grade FZ Si with SiO_2-SiN_x passivation

In this work, we proposed that charged hydrogen within the dielectric double layer would migrate under the influence of an electric field. The previous section has shown evidence of a strong dependence of surface passivation on the polarity of a surface electric field, with some conditions providing noticeable improvements. However, such gains can arise from enhanced chemical and field-effect passivation. The relative importance of these two effects is considered in the following.

An examination of the interface parameters was conducted by using a semi-transparent PEDOT:PSS gate biasing experiment [30,61]. In this experiment, the surface recombination at the interface is controlled by regulating the carrier density via field effect. The dependence of effective lifetime for an incremental sweep in surface voltage biases is recorded, identifying the minimum effective lifetime of each sample, as depicted in Fig. 3 a. Samples from group A that had (i) as deposited SiO_2-SiN_x, (ii) SiO_2-SiN_x annealed for 20 s at 450 °C in air, (iii) positive corona (30 s) annealed (450 °C 20 s) SiO_2-SiN_x, and (iv) negative corona (30 s) annealed (450 °C 20 s) SiO_2-SiN_x, were analysed. The minimum recorded lifetime is directly related to the capture velocities of electrons and holes for this Si–SiO_2 interface. We note that this data set has been previously reported in Ref. [44], yet we include here a new analysis and understanding of these results as follows.

The solid lines in Fig. 3 a illustrate a theoretical model of effective lifetime using an extended Shockley-Read-Hall formalism with the parametrisations in Ref. [35], as detailed in the Supplementary Materials. The values used for all parameters required to model this experimental data are included in Table S2. Most notably, this parameterisation uses the capture velocities for electrons and holes (S_{n0}, S_{p0}), and the concentration of fixed dielectric charge Q_f to predict the overall lifetime observed on each sample. The minority carrier capture velocity S_{p0} and the fixed dielectric charge Q_f are plotted on Fig. 3 b.

These results show that the positive corona-anneal provides additional field-effect passivation, as evidenced by increases in dielectric fixed charge (Q_f). This finding has also been corroborated using capacitance-voltage measurements as detailed in the Supplementary Materials, Fig. S3. The charge concentration required in the gate to correctly model the observed lifetime behaviour is 5×10^{11} q cm^{-2}. This charge concentration is higher than that intrinsically obtained in the PECVD SiN_x films (3×10^{11} q cm^{-2}), yet much lower than typically reported in the literature where 10^{12} q cm^{-2} is achieved [62,63]. This, therefore, highlights the potential of extrinsic processes that exploit the surface passivation dielectrics by increasing stored charge.

Results in Fig. 3 a also show that the chemical passivation is affected by a surface electric field during firing. In the control case, where the SiN_x-SiO_2 double layer is expected to have some positive charge already, S_{p0} reduces by one third. However, under additional positive corona charge, that reduction in S_{p0} is not as pronounced (Fig. 3 b and Table S1). Conversely, a negative electric field on the surface severely impacts the chemical passivation obtained after firing with S_{p0} increasing by 7 times. The observed changes in chemical passivation indicate three possible mechanisms. First, changes can occur in the density of recombination-active mid-gap interface sates (D_{it-mg}) leading to a reduced capture rate. Second, a reduction in the capture cross-section of holes σ_p at interface states is possible, since the fundamental hole capture rate is given by $S_{p0} = v_{th}\sigma_p D_{it}$, with D_{it} representing the energy-dependent interface state density, and v_{th} the carrier's thermal velocity. Lastly, if H passivation of interface states is involved during corona anneals, it is possible that the state's energy level within the bandgap is modified, thus changing their recombination activity. This distinction is not possible in the general model considered here, yet similar observations have been made by the passivation of H to bulk metal impurities in silicon [64–66]. Overall, the interface parameters extracted are in good agreement with those reported for this passivation stack in previous work [35,67,68], with a key novel finding: the polarity of the dielectric charge influences not just the field effect but also the final chemical passivation obtained on the Si–SiO_2 interface after low temperature firing.

4.2. Industrial grade Cz Si with SiO_2-SiN_x passivation

Solar-relevant textured surfaces were also investigated to determine the effects that surface electric fields have on the final surface passivation properties of Si–SiO_2 interfaces. Group C specimens were used but instead annealed for 120 s at 450 °C in air, after 30s of positive or negative corona deposition. An additional C.4 SiO_2-SiN_x specimen was created with 60 s of negative corona charge applied to both surfaces followed by annealing at 450 °C for 120 s. This specimen is labelled as '2x Negative Corona, Anneal'. Previous work has shown that dielectric thin films on textured surfaces present a higher concentration of pinholes [69]. Hence, it was not possible to apply the transparent PEDOT:PSS gate to group C samples. Instead, corona discharge was used to regulate the surface carrier concentration (n_s and p_s). After processing both dielectric surfaces were biased with incremental additions of negative corona charge while τ_{eff} was recorded on the Sinton tester. Although Kelvin Probe can be used to measure the surface charge on a full-size 6-inch substrate, the dimensions of the instrument make it difficult to fit large specimens under the probe. To prevent damage to

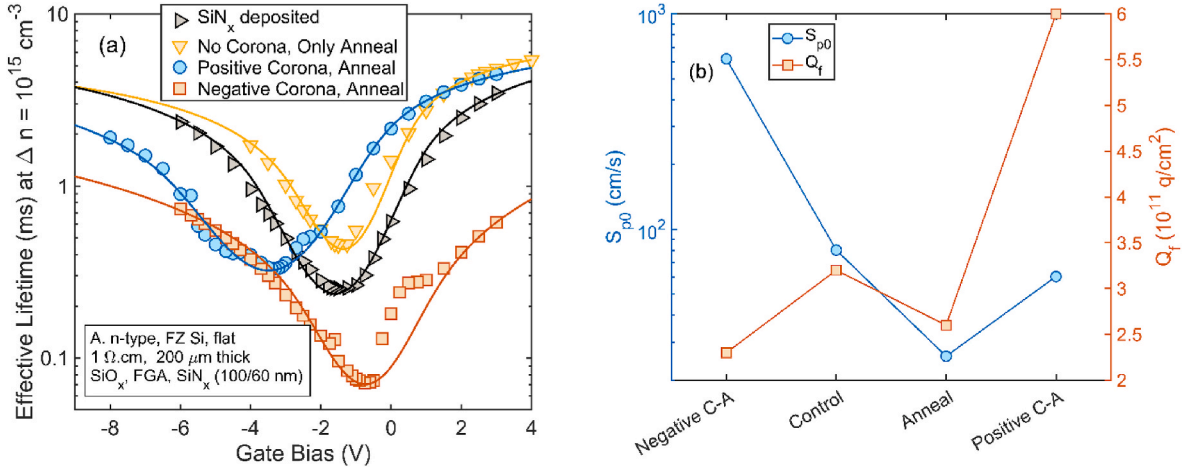

Fig. 3. (a) Effective lifetime as a function of gate bias for planar A specimens measured via the PEDOT:PSS transparent gate. Lines are model fittings using the energy-dependent S_{p0} and Q_f parameters schematically drawn in (b), and listed in Table S2. C-A refers to a corona-anneal.

the sample, 1 K Probe measurement was taken before depositing negative charge to determine the reference contact potential difference. A calibration was used to calculate the increases in charge from the measured surface potential, after each corona deposition following 5 s or 10 s charging periods (see the Supplementary Materials). The cycle of corona charging and Sinton lifetime testing was performed continuously to prevent artefacts from the dissipation of corona charge [45]. The whole experiment was completed within 90 min. The resulting lifetime versus surface charge relationships are illustrated in Fig. 4 a.

The solid lines in Fig. 4 a indicate the best fitting obtained for these group C specimens after processing and measurement. The detailed parameters are provided in the Supplementary Materials, Table S3. The most relevant parameters, S_{p0}, Q_f, are illustrated in Fig. 4 b. Here it is clear that annealing the industrial SiO_2-SiN_x passivated specimens without an extrinsic electric field result in degradation of the chemical passivation evidenced in the increased S_{p0}. This contradicts the observations for research grade FZ Si in Section 4.1. Relative to the as-deposited SiO_2-SiN_x control, S_{p0} increased by approximately ten times. Annealing the dielectric stack in the presence of an extrinsic positive field resulted in poorer levels of chemical passivation, despite a clear increase in field effect passivation as evidenced by the increased Q_f. On the other hand, applying a negative surface field prevented the chemical degradation, compared to the original SiO_2-SiN_x control. Since negative charge seemed to have an important effect, we processed an additional sample with higher negative electric field intensity. The '2x negative corona, anneal' specimen resulted in the best quality interface out of all 5 specimen types processed. Relative to the as-deposited control, S_{p0} remained at approximately the same value providing excellent surface passivation, despite the smaller field effect component ($Q_f \sim 1.5 \times 10^{12}$ q cm^{-2}).

The results of Group A and Group C samples demonstrate that the surface electric field influences the chemical passivation of the interface. However, the mechanisms by which the interface properties change in Group A appear to be different than in Group C. In Group A, the negative electric field during annealing degrades the interface passivation. In contrast, for Group C negative surface fields during annealing showed improvements in the chemical passivation of the interface. To ensure that these effects where completely reproducible, the experiment in Fig. 4 was repeated and the intensity of the electric fields varied. The results of such experiment are included in the Supplementary Fig. S4 and Table S6, showing that the findings are completely reproducible and highly dependent on the electric field.

A key difference between the two types of specimens is the properties of the SiN_x dielectric. Starting with the intrinsic concentration of charge, the research grade PECVD contains much less charge than industrial PECVD SiN_x. The density, stoichiometry, and structure (including H content) in the SiN_x films also influence the desorption and mobility of hydrogen [70–72]. Most often such chemical and structural changes in SiN_x are monitored via the film's refractive index. Bredemeier et al. reported that the in-diffusion and out-diffusion of hydrogen at the silicon interface were predominantly influenced by the SiN_x film properties closest to the interface [71]. High refractive index (low density) films, for example, have a greater tendency to release dimers rather than atomic hydrogen [70,71]. To determine whether the nitride properties explain the difference in the observations, the effect of surface electric fields on the chemical properties was studied on films with three different refractive indices, and H desorption was enhanced by annealing at a higher temperature of 600 °C.

The density and stoichiometry of the SiN_x was varied by regulating the silane to ammonia precursor gases, leading to films with n = 1.95, 2.1, and 2.4. The refractive index is known to vary due to stoichiometry and increases with greater silicon density. The intrinsic film charge also depends upon film composition and increases with increased nitrogen content due to the formation of K-centres [73]. For each refractive index, 3 types of specimens were produced: a control with no further processing, a substrate that was annealed at 600 °C in the presence of a 60 s positive corona field, and a substrate that was annealed at 600 °C in the presence of a negative corona field. The results of the surface-biased lifetime experiment are shown in Fig. 5. The interface recombination modelling parameters are given in Table S4. Fig. 5 a compares the results for three group C specimens where the SiN_x refractive index was 1.95. Annealing in the presence of a positive surface field resulted in a significant reduction in chemical passivation, as seen by a lifetime minima 100 μ s lower than the control, which resulted from an increase in S_{p0} by 20-fold. In contrast, annealing in the presence of a negative surface field improved the interface. Relative to the control, the S_{p0} reduced by half. Fig. 5 b shows the results for a refractive index of 2.1. A similar pattern was observed as in Fig. 5 a, however, here the degradation due to positive surface fields was less stark. The positively charged sample showed a smaller increase in S_{p0} by tenfold. Annealing in the presence of a negative surface field showed a reduction in S_{p0}. Fig. 5 c shows the results for the highest refractive index of 2.4. Here, the hole capture rate did not vary substantially for the positively charged sample, compared to the control. The sample that was negatively charged again showed an improvement in the chemical passivation. The S_{p0} lowered by a factor of ten. These results show that the refractive index affects the mechanism

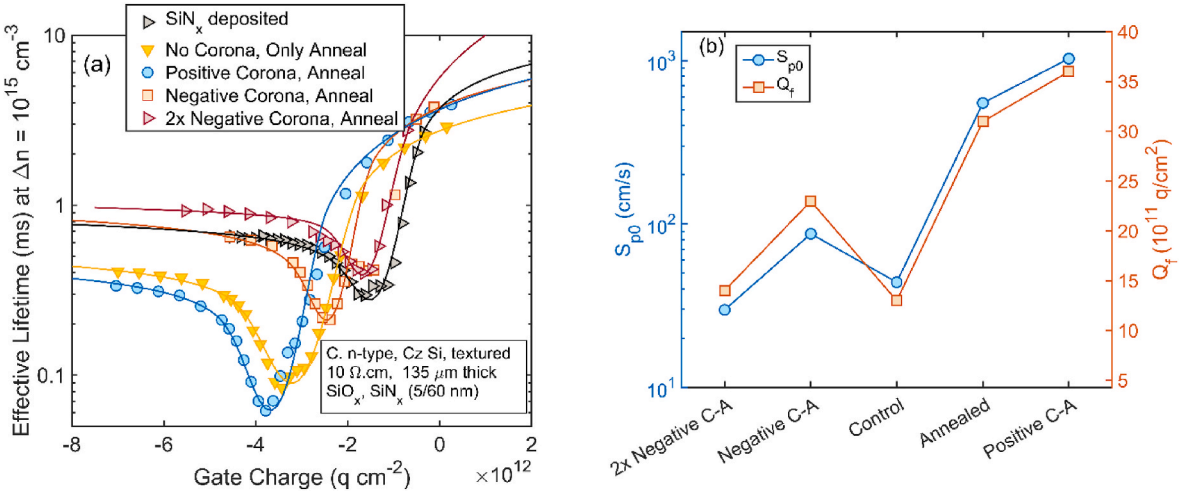

Fig. 4. (a) Effective lifetime as a function of equivalent surface charge for textured type C specimens with n = 1.95 SiN_x, measured via subsequent deposition of corona discharge. Lines are model fittings using the energy-dependent S_{p0} and Q_f parameters as schematically drawn in (b), and listed in Table S3. Group C samples with 5/60 nm SiO_2-SiN_x. C-A refers to a corona-anneal.

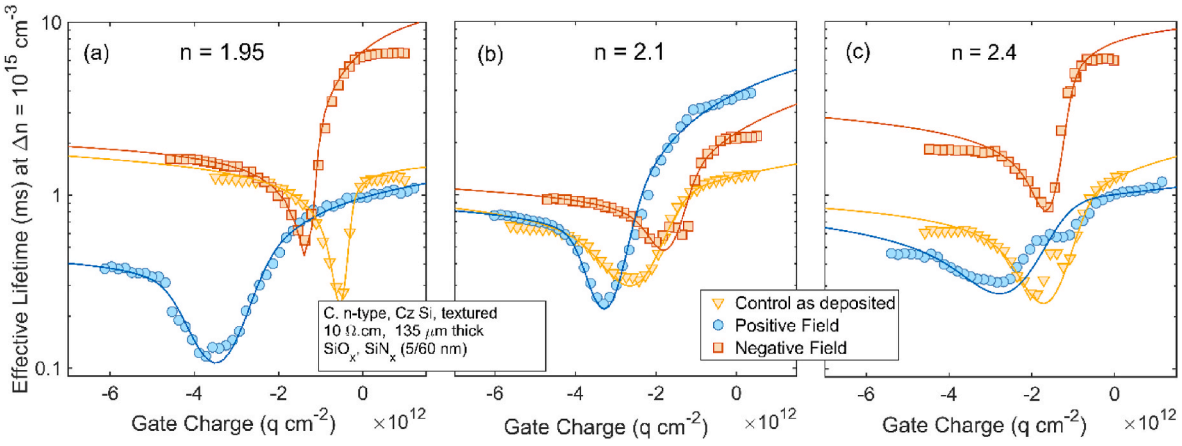

Fig. 5. Effective lifetime as a function of equivalent surface charge for textured type C specimens with SiO_2/SiN_x passivation stack, where the nitride had (a) n = 1.95, (b) n = 2.1, (c) n = 2.4 refractive index. The surface population was controlled via subsequent deposition of corona discharge. Solid lines are model fittings using the energy-dependent S_{p0} and Q_f parameters and listed in Table S4.

by which surface polarisation changes the chemical interface properties. This is particularly evident for samples annealed in the presence of a positive surface field. The detrimental effect of the positive polarisation is minimised as the refractive index increases and more H is available as reported in Ref. [71]. In all cases, annealing in the presence of a negative surface field improves the interface passivation. The results in Fig. 5 do not provide an explanation of the contrasting observations for Group A specimens where the refractive index of the SiN_x film was 1.9. It is therefore hypothesised that the passivation or de-passivation mechanism is not solely related to the dielectric density or hydrogen content. A discussion of various possible passivation mechanisms is presented in Section 5.

4.3. *Industrial grade Cz Si with SiO_2 passivation*

In this work, we hypothesised that hydrogen can be driven in and out of the Si–SiO_2 interface after its desorption from a SiN_x layer and field-induced migration. Section 3 showed that, in research-grade specimens, the presence of H inside the SiO_2 obtained via FGA was fundamental in achieving outstanding passivation. The question arises to what extent the H already present inside the SiO_2 can be electrostatically manipulated, making the SiN_x film unnecessary for the observed interface passivation effects. To address this, we test Group C.1 substrates with a 5 nm SiO_2 dielectric on both surfaces, without a SiN_x film. We use Group C as it is the most industrially relevant processed oxide. The oxide surfaces were positively or negatively charged (30 s), then annealed at 450 °C for 2 min. The results of the subsequent surface-biased lifetime experiment on these samples are provided in Fig. 6. The interface recombination parameters used to fit the data to a theoretical model are given in the Supplementary Materials, Table S5. From Fig. 6 a it is clear that the as-oxidised interface is highly recombination active. The modelled S_{p0} was 3×10^3 cm/s before any processing which is over two orders of magnitude higher than with SiN_x deposited. This highlights the importance of chemical passivation induced by the nitride, now well agreed to originate from the presence of hydrogen and broadly exploited in the research and industrial communities [74]. Annealing without any extrinsic electric field did not significantly alter the interface properties. Annealing the control with a positive surface field resulted in an unexpected improvement to the interface properties as the S_{p0} reduced by a third. Additionally, a slight increase in the dielectric's positive charge was detected. Annealing in the presence of negative surface electric fields also demonstrated improvements in chemical passivation. The S_{p0} decreased by 30 %. Another unexpected finding was a sixfold increase in positive charge within the oxide film when the sample was annealed after negative corona deposition, as evidenced by the greater shift along the negative x-axis, and the modelled Q_f parameter in Fig. 6 b. To ensure

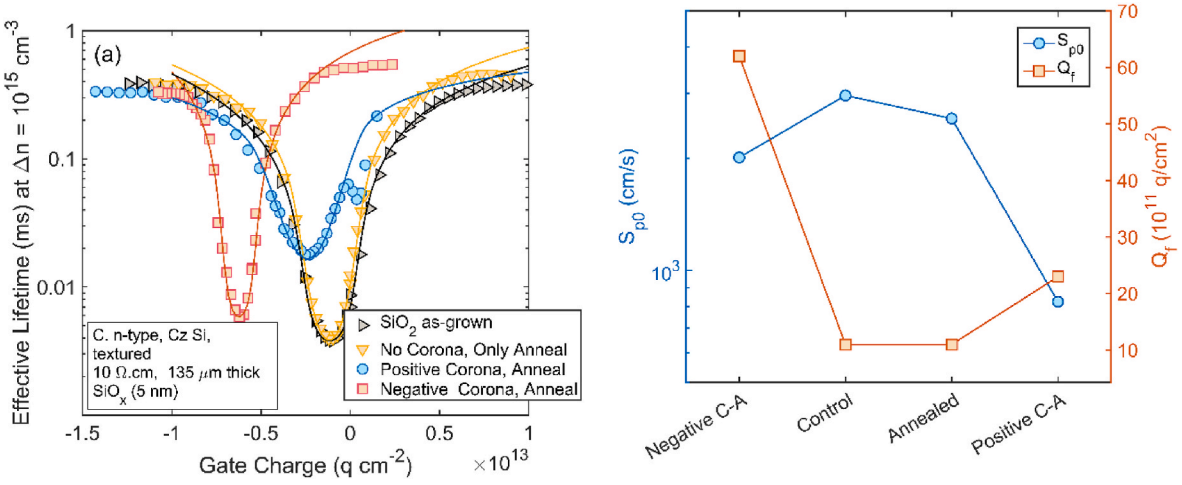

Fig. 6. (a) Effective lifetime as a function of equivalent surface charge for textured type C.1 specimens with 5 nm SiO_2 passivation on both surfaces, measured via subsequent deposition of corona discharge. Lines are model fittings using the energy-dependent S_{p0} and Q_f parameters as schematically drawn in (b), and listed in Table S4. C-A refers to a corona-anneal.

these results are reproducible and indicative of a trend, a fresh second set of specimens was produced that underwent identical positive and negative surface charging before annealing. The repeated surface-biased lifetime results are consistent with those in Fig. 6, and are included in the Supplementary Materials, Fig. S5. Overall, these results show that an electric field can also influence the chemical passivation on single-layer SiO_2, yet to a much smaller extent than in the presence of SiN_x. In alignment with the results for research grade specimens in Section 4.1, the interface improved upon positive corona annealing. More surprising was the fact that a high concentration of positive charge was embedded in the oxide film due to the annealing under a *negative electric field*. All results in Section 4 are next discussed in depth.

5. Discussion

Our work originates from the premise that hydrogen is primarily a charged species inside dielectric thin films, and thus its migration must respond to electrostatic stimuli. While it is impossible to ascribe all the changes in chemical passivation directly to hydrogen, the results presented in Section 4 indicate that the obtained passivation at Si–SiO_2 interfaces depends on the intensity and polarity of an electric field. We therefore propose arguments for how H migration could account for the observed behaviours. Numerous reports exist concerning the role of hydrogen in silicon surface passivation. However, the mechanism of hydrogen passivating interface defects is still under debate [6,75–77]. The general observations in the field indicate that dangling bonds at the Si–SiO_2 interface can be passivated by both molecular and atomic forms of hydrogen [13,20,78,79]. Atomic hydrogen has been reported to both passivate dangling bonds [20,80], or be responsible for de-passivation.

It is widely reported that H^+ is the predominant charge state within SiO_2 generated through a reaction between holes and hydrogen [13,20, 24,79]. The positive charge state is highly stable owing to the considerably higher energy level of H^+ compared to the conduction band of silicon, which minimises the probability of neutralisation by electron injection [13,20,24]. In addition to H^+, neutral H^0 has also been reported to remain stable and passivate defects at the Si–SiO_2 interface [80,81]. Lastly, some experimental studies show that dimers can also passivate silicon dangling bonds at the Si–SiO_2 interface [13,79,82–84].

The passivation and de-passivation mechanisms occur spontaneously with a very small energy barrier [80]. Stathis et al. reported a greater probability of the passivation mechanism occurring than the de-passivation [80]. The activation energies associated with both mechanisms are reported to have little dependency on surface orientation [79,85]. In the case of a textured (111) Si–SiO_2 interface, passivation by H_2 can be defined by a single activation energy of 1.66 eV [79, 82,85]. At a planar (100) face, the passivation activation energy is reported to range between 1.51 eV and 1.6 eV [79,86,87]. The activation energy of the de-passivation mechanism is ~2.6 eV for both (111) and (100) orientations [80,88]. Therefore, the behaviour of hydrogen is not expected to depend upon the interface orientation significantly. The primary difference between the two orientations is the density of electrically active defects present and the intrinsic positive interface charge. At the (100) Si–SiO_2 interface, there are significantly fewer defects created than at (111) interfaces [89,90], resulting in a lower concentration of trapped positive holes.

With these mechanisms in play, we now refer to the observations in Section 4, starting with the electrostatics occurring at single-layer SiO_2 film under a biased anneal. The results in Section 4.3 lead to three key conclusions. Firstly, there is an improvement in the interface properties upon annealing in the presence of both positive and negative surface electric fields. The observed improvements in chemical passivation can be explained by the capturing of the residual hydrogen in the oxide, regardless of the field. It is known that hydrogen can be introduced to SiO_2 by water molecules [91,92], and through ions generated by corona discharge [93]. It is therefore not possible to assume zero hydrogen within the system by eliminating the SiN_x capping layer. However, the SiN_x layer is critical in achieving high passivation levels with the minority capture rate decreasing by over two orders of magnitude. This corroborates widely known observations of H passivation thanks to nitride films.

Secondly, when annealing in the presence of a positive charge, corona ions can inject their charge into the SiO_2 thin film. However, the total injected positive charge is only a fraction of that placed on the film's surface via corona. This means that either the positive charge injection is not as efficient as the corona leakage mechanisms reported in previous work [45], or that some of the corona charge injected gets quickly neutralised by the injection of hot electrons from the silicon conduction band [21]. Looking at the lifetime versus gate charge curve in Fig. 6 a, it appears that an additional defect in the upper half of the bandgap is created. This is evidenced by the dip in τ_{eff} at a gate charge of $\sim+10^{11}$ q cm^{-2}. This newly generated defect is reproducible as seen by the repeated surface-biased lifetime results in the Supplementary Materials, Fig. S5. In fact, this defect is also present in other experiments. To aid understanding, corona-annealed Si–SiO_2 interfaces which show such defects have been displayed in Fig. S6. It is therefore likely that hot electron injection is responsible for the extra interface defects as also found in previous works [21]. We suggest future work can use the X-ray photoelectron spectroscopy to elucidate changes in structural properties of the Si–SiO_2 interface. Previous work has shown such method practical in identifying chemical composition and oxidation states at the interface [28,94], which could provide information about the observed defect.

Thirdly, annealing the oxide in the presence of a negative surface increases the positive charge inside the dielectric. Such accumulation of positive dielectric charge after depositing negative corona charge on SiO_2 has been previously reported in Refs. [95–97]. It is believed that the positive charge arises from hole trapping reported to exist in high concentrations at the Si–SiO_2 interface, and are predominantly attributed to strained interfacial bonds [95–99]. Hole trapping can occur through three primary mechanisms: (i) Through the emission of an electron from a neutral state to the conduction band of SiO_2, which leaves behind a hole [96]. Electron emission from such traps is reported to be the predominant mechanism of creating trapped holes. (ii) Hot hole injection from the silicon to the SiO_2 [100,101]. This mechanism becomes more likely with increasing negative field strength to overcome the valence band offset between silicon and SiO_2. (iii) Direct tunnelling of an electron from a neutral centre to the conduction band of silicon, which leaves behind a positively charged hole trap [96]. This mechanism is dependent upon the alignment of the energy levels and is restricted to trap centres in very close proximity to the interface [96]. Once the electric field is removed, carriers can tunnel back, and thus this mechanism is unlikely. In Fig. 6 a. a positive dielectric charge exists even after the negative corona charge has decayed from the annealing. Mechanisms (i) and (ii) are likely in play.

We now focus on the results for sample sets A and C with a nitride present, Sections 4.1 and 4.2. In the case of group A specimens, a positive surface electric field leads to enhanced field effect passivation yet only at a Q_f ~5×10^{11} q cm^{-2}. A marginal improvement to chemical passivation is seen since S_{p0} reduces, yet not to the same extent as the control annealed sample without extrinsic corona fields. Negative electric fields, on the other hand, produce large interface chemical degradation as well as a small decrease in field-effect passivation. In group C specimens, a contradictory trend was observed. At annealing temperatures of both 450 and 600 °C positive surface fields resulted in degradation of the chemical properties, and negative surface fields resulted in improvements. It is clear that surface electric fields influence the chemical passivation properties of the interface. However, it appears that the mechanisms at play are different between specimens in groups A and C. We now attempt to reconcile the findings by proposing a series of H-related and charge injection processes that play a role in the observed results.

A schematic picture of all mechanisms is given in Fig. 7. Starting with group A specimens, we note that a D_{it} in the order of 10^{10}-10^{11} cm^{-2}

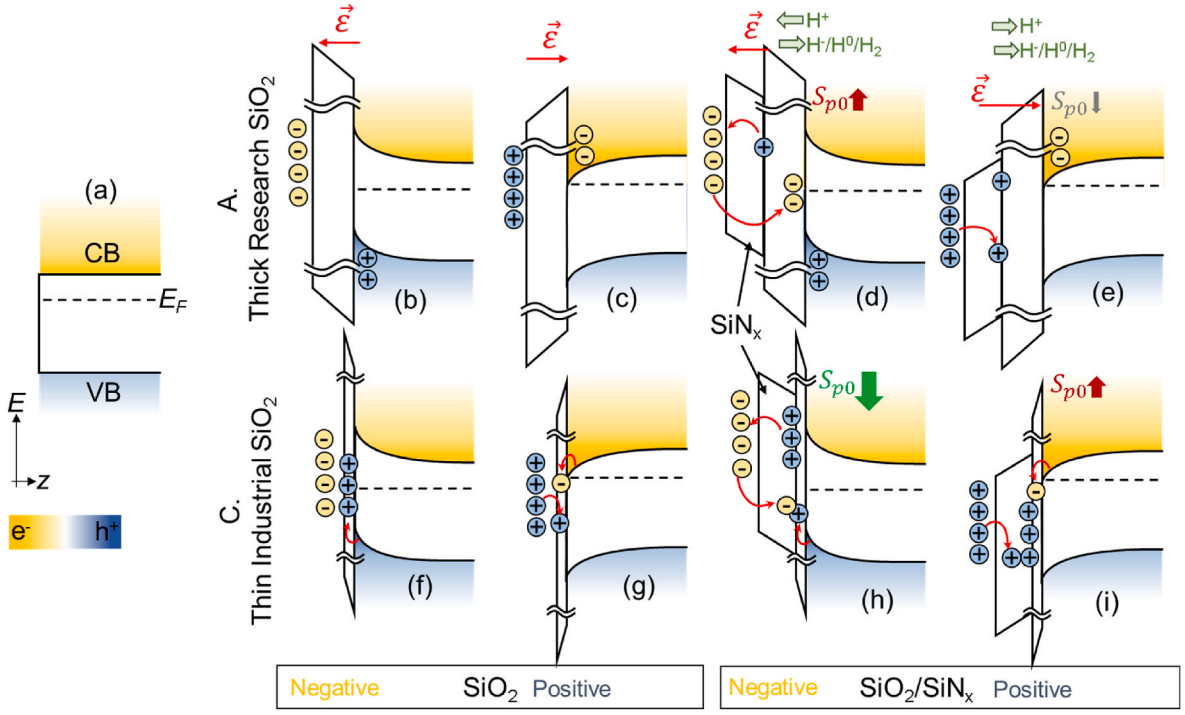

Fig. 7. Schematic diagram of the mechanisms of charge and hydrogen interaction at Si–SiO2 interfaces, with and without the presence of a nitride capping layer. (a) The bare system of an n-type Si surface. Group A Si–SiO_2 interface under a negative (b) and positive (c) surface electric field from corona ions. Group A Si–SiO_2-SiN_x interface under a negative (d) and positive (e) surface electric field from corona ions. Group C Si–SiO_2 interface under a negative (b) and positive (c) surface electric field from corona ions. Group C Si–SiO_2-SiN_x interface under a negative (d) and positive (e) surface electric field from corona ions.

eV^{-1} is expected in as-grown Si–SiO_2 interface due to the low defect density in (100) surfaces [35,102]. Additionally, the oxide film was subjected to a forming gas anneal, which is well-reported to introduce significant quantities of hydrogen [58,92,103]. It is then proposed that the Si–SiO_2 interface was very well passivated by the hydrogen introduced during the FGA and nitride deposition. The hypothesised mechanisms are illustrated in Fig. 7b-e. Here, it is proposed that H^+ and H^- drifted towards or away from the interface under the influence of electric fields. Neutral atomic and molecular forms may also diffuse under high temperatures towards the interface. For group A samples, due to the excellent pre-existing passivation, the additional hydrogen migration does not impact passivation further. Under a positive electric field, the charging of defects at the SiO_2-SiN_x interface results in small additional positive Q_f and better FEP (Fig. 7e). Annealing under negative surface electric fields (Fig. 7d) leads to heavy depassivation. It is possible that the pre-existing hydrogen is thermally dissociated from interface defect sites, likely due to electron injection from the SiN_x surface, thanks to the corona ions conceding their charge. In fact, when examining Fig. 3 a in detail, it is clear that a defect appears for a gate bias of ~ 0–1 V, leading to a decrease in τ_{eff}. This is the same defect identified earlier as originating from electron injection into the Si–SiO_2 interface and is also displayed in Fig. S6 for clarity.

Let us now concentrate on group C specimens, Fig. 7f-i. Here, we observe two key findings when the SiO_2 film is polarised without a SiN_x capping layer. Under negative electric fields, mild hydrogenation occurs, possibly as H^- species are dragged to the interface. This occurs as holes are injected from the silicon surface into the oxide, which build a positive Q_f and provide field effect passivation (Fig. 7f). Under positive electric fields (Fig. 7g), there appears to be a component of electron injection from the Si surface which causes degradation via an upper-midgap defect. Yet, substantial H passivation occurs from H+ migration into the interface, overall resulting in an improved chemical interface.

Consider now the case where SiN_x is present in group C specimens. Improved chemical passivation is achieved purely due to the nitride deposition. Then, annealing under a negative electric field leads to little change in the chemical interface, with a small hydrogenation improvement arising, presumably from $H^-/H^0/H_2$ species reaching the interface. The negative electric field also prevents the SiO_2-SiN_x film from gaining a net positive charge. This can occur due to two factors: electrons get injected from the corona ions into the dielectrics, neutralising the formed positive charge; or the negative electric field inhibits the processes by which traps in the dielectric become positively charged. It is more plausible that the former mechanism is the primary contributor as the final positive Q_f reduces in magnitude, the higher the negative corona ion concentration. Additionally, as occurred in the SiO_2 single-layer case, it is possible that some holes are injected from the silicon into the oxide. Still, such holes do not remain charged as the final Q_f is positive but lower in magnitude when the nitride is present during negative corona annealing.

Annealing the SiO_2-SiN_x in group C under a positive electric field leads to a surprising degradation of the chemical interface, observed in a marked increase of S_{p0}. The main mechanism believed to be at play is the injection of hot electrons from the Si into the Si–SiO_2 interface. The role of electron injection in de-hydrogenation of the interface is reported in Refs. [24,104,105]. Such injection is enhanced by the intrinsic positively charged defects in the SiO_2-SiN_x and the added positive surface corona ions. The intrinsic defects in the SiO_2-SiN_x seem to govern the final concentration of positive charge, as the corona ions do not increase the final positive Q_f, observed to be around 3–4 × 10^{12} q cm^{-2}.

In light of these hypothesised mechanisms, the role of negative charge is primarily to prevent the injection of electrons from the Si surface into the SiO_2, thus preventing the degradation of the chemical passivation in group C. It is also possible that, under a sufficiently high negative electric field, holes from the Si are injected into the SiO_2 and can react with H species ($H^0 + h \rightarrow H^+$), promoting passivation as reported in Ref. [106]. Overall, with a negative corona anneal mild passivating effects can occur via $H^0/H^2/H^-$, without the detrimental

effects of electron injection as the silicon surface is now hole-rich.

The main difference between groups A and C seems to be the possibility of hot carrier injection from the Si surface space charge. In research-grade thicker SiO_2, such a process seems to be inhibited by a superior Si–SiO_2 interface. In the lower temperature and fast-throughput industrial SiO_2, the initial interface is clearly inferior and thus benefits from H passivation. The lifetime data for samples An under negative corona anneal and samples B under positive corona anneal indicate that hot electrons are detrimental and can lead to depassivation of the interface. An electron-induced defect is observed in both cases, with high activity near the mid-upper bandgap region, Fig. S6.

We note here that previous work by Jin et al. used a comparable experimental approach and revealed analogous surface-biased lifetime dependencies of hydrogenated Si–SiO_2 structures [93]. They reported interface degradation under both low positive and negative surface field conditions, which they attributed to both the depassivation of silicon dangling bonds, and the generation of new defects by atomic hydrogen [93]. Contrary to the observations of Jin et al., there is no evidence of interface degradation for positive surface fields on group A specimens. Additionally, it was found that the passivation performance is improved in the case of group C specimens when they are negatively charged before annealing. It is proposed here that the dynamics of hydrogen and charge injection across the oxide-silicon interface are responsible for the observed changes in chemical passivation.

We finally turn our attention to group C samples, where the refractive index of the nitride is varied. The specimens in Fig. 5 c show a clear trend based on the refractive index of the SiN_x film. Increasing the refractive index reduces the detrimental effect of positive surface fields during annealing. At the highest refractive index of 2.4, there was a negligible difference between the chemical passivation of the interface for the control specimen and the positively charged specimen. It is well-reported that hydrogen content within SiN_x increases with increasing refractive index [71,72]. Bredemeier et al. reported that the maximum hydrogen concentration is desorbed in films where n = 2.4 [71]. It is hypothesised here that regardless of the field polarity, hydrogen is drifted or diffused to the silicon surface where it passivates dangling bonds. For group C specimens with the lowest n of 1.95, hydrogen-terminated dangling bonds are de-passivated by electron injection, similarly to the mechanism presented in Fig. 7 i. With increasing refractive index, the substantially higher concentration of available hydrogen swiftly passivates previously de-passivated dangling bonds, thus overriding the de-passivation mechanism by electron injection. This effect is most evident in specimens with a refractive index of 2.4, which are believed to have the greatest hydrogen concentration. It was also shown that irrespective of film density, annealing group C specimens in the presence of negative surface fields improved chemical passivation substantially, via the mechanisms previously suggested: inhibition of detrimental electron injection, injection of holes, and migration of H_0/H_2.

6. Conclusions

This work demonstrates that:

1. Hydrogen passivation is pivotal in improving silicon solar cell performance via reduced surface recombination, and hydrogenated dielectrics are crucial to cell manufacturing.
2. The chemical passivation of Si–SiO_2-SiN_x interfaces is dependent on the polarity and strength of the surface electric field.
3. A distinct difference in passivation quality is obtained after elevated temperature firing when positive or negative corona charge is deposited on the dielectric surface, with optimal processing being dependent on the surface electric field, the oxide-silicon interface quality, and the nitride hydrogenation and charge migration properties.
4. The dielectric hydrogen content (presumed to be determined by the refractive index) influences passivation effectiveness, with higher refractive indices enhancing hydrogen passivation.
5. Understanding the interplay of hydrogen and electric fields is crucial for optimising silicon solar cell performance.

Additionally, we have shown that passivation can be improved to >1 ms lifetimes on textured wafers, after optimal corona charging and medium temperature annealing. The best passivation quality achieved shows an SRV< 1 and 5.6 cm/s for research- and industry-grade specimens respectively, which equate to a $J_{0s} < 15$ fA cm^{-2} without correcting for the higher surface areas. The possibility of controlling the hydrogenation of a silicon solar cell can have extensive implications for future improvements in device performance, and industrial deployment of controlled hydrogenation.

CRediT authorship contribution statement

Ruy S. Bonilla: Writing – review & editing, Writing – original draft, Methodology, Investigation, Funding acquisition, Formal analysis, Data curation, Conceptualization. **Isabel Al-Dhahir:** Writing – review & editing, Writing – original draft, Methodology, Investigation, Conceptualization. **Xinya Niu:** Investigation, Formal analysis. **Pietro P. Altermatt:** Writing – original draft, Methodology, Conceptualization. **Phillip Hamer:** Methodology, Investigation, Conceptualization.

Declaration of competing interest

The authors declare the following financial interests/personal relationships which may be considered as potential competing interests: RS Bonilla reports financial support was provided by Royal Academy of Engineering. RS Bonilla reports financial support was provided by UK Engineering and Physical Sciences Research Council. If there are other authors, they declare that they have no known competing financial interests or personal relationships that could have appeared to influence the work reported in this paper.

Data availability

Data will be made available on request.

Acknowledgments

All the authors are thankful to Radka Chakalova for assistance in clean-room processing. R.S.B was supported by the Royal Academy of Engineering under the Research Fellowship scheme (RF\201819\18\38). This work was supported by the UK Engineering and Physical Sciences Research Council (EPSRC) grant number EP/V038605/1, the International Engagement Fund from the SUPERGEN SuperSolar Plus network, and by the Oxford University John Fell Fund. For the purpose of Open Access, the author has applied a CC BY public copyright license to any Author Accepted Manuscript (AAM) version arising from this submission.

Appendix A. Supplementary data

Supplementary data to this article can be found online at https://doi.org/10.1016/j.solmat.2024.112799.

References

[1] D.M. Powell, M.T. Winkler, H.J. Choi, C.B. Simmons, D.B. Needleman, T. Buonassisi, Crystalline silicon photovoltaics: a cost analysis framework for determining technology pathways to reach baseload electricity costs, Energy Environ. Sci. 5 (2012) 5874, https://doi.org/10.1039/c2ee03489a.
[2] N.M. Haegel, P. Verlinden, M. Victoria, P. Altermatt, H. Atwater, T. Barnes, C. Breyer, C. Case, S. De Wolf, C. Deline, M. Dharmrin, B. Dimmler, M. Gloeckler,

J.C. Goldschmidt, B. Hallam, S. Haussener, B. Holder, U. Jaeger, A. Jaeger-Waldau, I. Kaizuka, H. Kikusato, B. Kroposki, S. Kurtz, K. Matsubara, S. Nowak, K. Ogimoto, C. Peter, I.M. Peters, S. Philipps, M. Powalla, U. Rau, T. Reindl, M. Roumpani, K. Sakurai, C. Schorn, P. Schossig, R. Schlatmann, R. Sinton, A. Slaoui, B.L. Smith, P. Schneidewind, B.J. Stanbery, M. Topic, W. Tumas, J. Vasi, M. Vetter, E. Weber, A.W. Weeber, A. Weidlich, D. Weiss, A.W. Bett, Photovoltaics at multi-terawatt scale: Waiting is not an option, Science 380 (1979), https://doi.org/10.1126/science.adf6957, 2023.

[3] M.A. Green, Commercial progress and challenges for photovoltaics, Nat. Energy 1 (2016) 15015, https://doi.org/10.1038/nenergy.2015.15.

[4] J. Schmidt, R. Peibst, R. Brendel, Surface passivation of crystalline silicon solar cells: present and future, Sol. Energy Mater. Sol. Cell. 187 (2018) 39–54, https://doi.org/10.1016/j.solmat.2018.06.047.

[5] A.G. Aberle, Surface passivation of crystalline silicon solar cells: a review, Prog. Photovoltaics Res. Appl. 8 (2000) 473–487, https://doi.org/10.1002/1099-159X(200009/10)8:5<473::AID-PIP337>3.0.CO;2-D.

[6] J. Schmidt, M. Kerr, A. Cuevas, Surface passivation of silicon solar cells using plasma-enhanced chemical-vapour-deposited SiN films and thin thermal SiO 2/plasma SiN stacks, Semicond. Sci. Technol. 16 (2001) 164–170, https://doi.org/10.1088/0268-1242/16/3/308.

[7] A. Cuevas, Y. Wan, D. Yan, C. Samundsett, T. Allen, X. Zhang, J. Cui, J. Bullock, Carrier population control and surface passivation in solar cells, Sol. Energy Mater. Sol. Cell. 184 (2018) 38–47, https://doi.org/10.1016/j.solmat.2018.04.026.

[8] J. Schmidt, F. Werner, B. Veith, D. Zielke, S. Steingrube, P.P. Altermatt, S. Gatz, T. Dullweber, R. Brendel, Advances in the surface passivation of silicon solar cells, Energy Proc. 15 (2012) 30–39, https://doi.org/10.1016/j.egypro.2012.02.004.

[9] S.W. Glunz, D. Biro, S. Rein, W. Warta, Field-effect passivation of the SiO2Si interface, J. Appl. Phys. 86 (1999) 683–691, https://doi.org/10.1063/1.370784.

[10] R.S. Bonilla, P.R. Wilshaw, Potassium ions in SiO 2 : electrets for silicon surface passivation, J. Phys. D Appl. Phys. 51 (2018) 025101, https://doi.org/10.1088/1361-6463/aa9b1b.

[11] K.A. Collett, S. Du, G. Bourret-Sicotte, Z. Luo, P. Hamer, B. Hallam, R.S. Bonilla, P.R. Wilshaw, Scalable techniques for producing field-effect passivation in high-efficiency silicon solar cells, IEEE J. Photovoltaics 9 (2019) 26–33, https://doi.org/10.1109/JPHOTOV.2018.2872032.

[12] W. Soppe, H. Rieffe, A. Weeber, Bulk and surface passivation of silicon solar cells accomplished by silicon nitride deposited on industrial scale by microwave PECVD, Prog. Photovoltaics 13 (2005) 551–569, https://doi.org/10.1002/pip.611.

[13] E. Cartier, J.H. Stathis, D.A. Buchanan, Passivation and depassivation of silicon dangling bonds at the Si/SiO $_2$ interface by atomic hydrogen, Appl. Phys. Lett. 63 (1993) 1510–1512, https://doi.org/10.1063/1.110758.

[14] K.A. Collett, R.S. Bonilla, P. Hamer, G. Bourret-Sicotte, R. Lobo, T. Kho, P. R. Wilshaw, An enhanced alneal process to produce SRV< 1 cm/s in 1 $Ω$ cm n-type Si, Sol. Energy Mater. Sol. Cell. 173 (2017) 50–58.

[15] A.G. Aberle, T. Lauinger, R. Hezel, Remote PECVD silicon nitride—a key technology for the crystalline silicon PV industry of the 21st century, in: Proceedings of the 14th European Photovoltaic Solar Energy Conference, Barcelona, Spain, 1997, pp. 684–689, 30.

[16] A.G. Aberle, Overview on SiN surface passivation of crystalline silicon solar cells, Sol. Energy Mater. Sol. Cell. 65 (2001) 239–248, https://doi.org/10.1016/S0927-0248(00)00099-4.

[17] C. Boehme, G. Lucovsky, H loss mechanism during anneal of silicon nitride: chemical dissociation, J. Appl. Phys. 88 (2000) 6055–6059, https://doi.org/10.1063/1.1321730.

[18] E.A. Douglas, P. Mahony, A. Starbuck, A. Pomerene, D.C. Trotter, C.T. DeRose, Effect of precursors on propagation loss for plasma-enhanced chemical vapor deposition of SiN_x:H waveguides, Opt. Mater. Express 6 (2016) 2892, https://doi.org/10.1364/OME.6.002892.

[19] G. Dingemans, M.C.M. van de Sanden, W.M.M. Kessels, Influence of the deposition temperature on the c-Si surface passivation by Al[sub 2]O[sub 3] films synthesized by ALD and PECVD, Electrochem. Solid State Lett. 13 (2010) H76, https://doi.org/10.1149/1.3276040.

[20] S.T. Pantelides, S.N. Rashkeev, R. Buczko, D.M. Fleetwood, R.D. Schrimpf, Reactions of hydrogen with Si-SiO/sub 2/interfaces, IEEE Trans. Nucl. Sci. 47 (2000) 2262–2268, https://doi.org/10.1109/23.903763.

[21] L.E. Black, K.R. McIntosh, Defect generation at charge-passivated Si–SiO2 interfaces by ultraviolet light, IEEE Trans. Electron. Dev. 57 (2010) 1996–2004, https://doi.org/10.1109/TED.2010.2051199.

[22] C.G. Van de Walle, J. Neugebauer, Universal alignment of hydrogen levels in semiconductors, insulators and solutions, Nature 423 (2003) 626–628, https://doi.org/10.1038/nature01665.

[23] L. Tsetseris, X.J. Zhou, D.M. Fleetwood, R.D. Schrimpf, S.T. Pantelides, Dual role of fluorine at the Si–SiO2 interface, Appl. Phys. Lett. 85 (2004) 4950–4952, https://doi.org/10.1063/1.1825621.

[24] S.N. Rashkeev, D.M. Fleetwood, R.D. Schrimpf, S.T. Pantelides, Defect generation by hydrogen at the Si-SiO2 interface, Phys. Rev. Lett. 87 (2001) 165506, https://doi.org/10.1103/PhysRevLett.87.165506.

[25] P. Hamer, B. Hallam, R.S.S. Bonilla, P.P.P. Altermatt, P. Wilshaw, S. Wenham, Modelling of hydrogen transport in silicon solar cell structures under equilibrium conditions, J. Appl. Phys. 123 (2018) 043108, https://doi.org/10.1063/1.5016854.

[26] J. Chen, K. Ge, C. Zhang, J. Guo, L. Yang, D. Song, F. Li, Z. Xu, Y. Xu, Y. Mai, Vacuum-free, room-temperature organic passivation of silicon: toward very low recombination of micro-/nanotextured surface structures, ACS Appl. Mater. Interfaces 10 (2018), https://doi.org/10.1021/acsami.8b17379.

[27] X. Wang, X. Zhang, Y. Bai, W. Li, B. Chen, J. Guo, X. Yang, X. Yan, S. Wang, J. Chen, Development of passivating edge shingle modules with right cut, new loss evaluation and liquid-based edge passivation strategy, Sol. Energy Mater. Sol. Cell. 261 (2023), https://doi.org/10.1016/j.solmat.2023.112513.

[28] N.E. Grant, S.L. Pain, J.T. White, M. Walker, I. Prokes, J.D. Murphy, Enhanced surface passivation of subnanometer silicon dioxide films by superacidic treatments, ACS Appl. Energy Mater. 5 (2022) 1542–1550, https://doi.org/10.1021/acsaem.1c02935.

[29] M. Moynihan, C. O'connor, B. Barr, S. Tiffany, W. Braun, G. Allardyce, J. Rentsch, K. Birmann, In-line and vertical texturing of mono-crystalline solar cells, in: Conference Record of the IEEE Photovoltaic Specialists Conference, 2010, pp. 1028–1033, https://doi.org/10.1109/PVSC.2010.5614629.

[30] R.S. Bonilla, Controlling surface carrier density via a PEDOT:PSS gate: an application to the study of silicon-dielectric interface recombination, Sol. RRL (2018) 1800172, https://doi.org/10.1002/solr.201800172.

[31] Q. Feng, K. Du, Y.-K. Li, P. Shi, Q. Feng, Effect of annealing on performance of PEDOT:PSS/n-GaN Schottky solar cells, Chin. Phys. B 23 (2014) 077303, https://doi.org/10.1088/1674-1056/23/7/077303.

[32] B. Friedel, P.E. Keivanidis, T.J.K. Brenner, A. Abrusci, C.R. McNeill, R.H. Friend, N.C. Greenham, Effects of layer thickness and annealing of PEDOT:PSS layers in organic photodetectors, Macromolecules 42 (2009) 6741–6747, https://doi.org/10.1021/ma901182u.

[33] R.B.M. Girisch, R.P. Mertens, R.F. Dekeersmaecker, R.F. De Keersmaecker, Determination of Si-SiO2 interface recombination parameters using a gate-controlled point-junction diode under illumination, IEEE Trans. Electron. Dev. 35 (1988) 203–222, https://doi.org/10.1109/16.2441.

[34] R.S. Bonilla, I. Al-Dhahir, M. Yu, P. Hamer, P.P. Altermatt, Charge fluctuations at the Si–SiO2 interface and its effect on surface recombination in solar cells, Sol. Energy Mater. Sol. Cell. 215 (2020) 110649, https://doi.org/10.1016/j.solmat.2020.110649.

[35] R.S. Bonilla, P.R. Wilshaw, On the c-Si/SiO2 interface recombination parameters from photo-conductance decay measurements, J. Appl. Phys. 121 (2017) 135301, https://doi.org/10.1063/1.4979722.

[36] W. Shockley, W.T. Read, Statistics of the recombinations of holes and electrons, Phys. Rev. 87 (1952) 835–842.

[37] A. Kimmerle, J. Greulich, A. Wolf, Carrier-diffusion corrected J0-analysis of charge carrier lifetime measurements for increased consistency, Sol. Energy Mater. Sol. Cell. 142 (2015) 116–122, https://doi.org/10.1016/j.solmat.2015.06.043.

[38] H. Mäckel, K. Varner, On the determination of the emitter saturation current density from lifetime measurements of silicon devices, Prog. Photovoltaics Res. Appl. 21 (2013) 850–866, https://doi.org/10.1002/pip.2167.

[39] D.E. Kane, R.M. Swanson, Measurement of the emitter saturation current by a contactless photoconductivity decay method, in: Proc of the 18th IEEE Photovoltaic Specialists Conference, 1985, pp. 578–583.

[40] T. Niewelt, B. Steinhauser, A. Richter, B. Veith-Wolf, A. Fell, B. Hammann, N. E. Grant, L. Black, J. Tan, A. Youssef, J.D. Murphy, J. Schmidt, M.C. Schubert, S. W. Glunz, Reassessment of the intrinsic bulk recombination in crystalline silicon, Sol. Energy Mater. Sol. Cell. 235 (2022) 111467, https://doi.org/10.1016/j.solmat.2021.111467.

[41] PV LightHouse. www.pvlighthouse.com.au, 2022. Cells calculators.

[42] R. Pässler, Dispersion-related description of temperature dependencies of band gaps in semiconductors, Phys. Rev. B 66 (2002) 085201, https://doi.org/10.1103/PhysRevB.66.085201.

[43] B. Hammann, B. Steinhauser, A. Fell, R. Post, T. Niewelt, W. Kwapil, A. Wolf, A. Richter, H. Höffler, M.C. Schubert, Quantifying surface recombination - improvements in determination and simulation of the surface recombination parameter J0s, IEEE J. Photovoltaics 13 (2023), https://doi.org/10.1109/JPHOTOV.2023.3265859.

[44] I. Al-Dhahir, S. McNab, M. Yu, E. Shaw, P. Hamer, R.S. Bonilla, The influence of surface electric fields on the chemical passivation of Si-SiO2 interfaces after firing, AIP Conf. Proc. 2487 (2022) 130001, https://doi.org/10.1063/5.0089930.

[45] R.S. Bonilla, C. Reichel, M. Hermle, P. Hamer, P.R.P.R. Wilshaw, Long term stability of c-Si surface passivation using corona charged SiO2, Appl. Surf. Sci. 412 (2017) 657–667, https://doi.org/10.1016/j.apsusc.2017.03.204.

[46] R.S. Bonilla, N. Jennison, D. Clayton-Warwick, K.A. Collett, L. Rands, P. R. Wilshaw, Corona charge in SiO2: kinetics and surface passivation for high efficiency silicon solar cells, Energy Proc. 92 (2016) 326–335, https://doi.org/10.1016/j.egypro.2016.07.090.

[47] B. Stegemann, J. Kegel, M. Mews, E. Conrad, L. Korte, U. Stürzebecher, H. Angermann, Passivation of textured silicon wafers:influence of pyramid size distribution, a-Si:H deposition temperature, and post-treatment, Energy Proc. 38 (2013) 881–889, https://doi.org/10.1016/j.egypro.2013.07.360.

[48] N. Ximello, A. Dastgheib-Shirazi, S. Scholz, G. Hahn, Influence of pyramid size of chemically textured silicon wafers on the characteristics of industrial solar cells, 25th European Photovoltaic Solar Energy Conference and Exhibition, in: 5th World Conference on Photovoltaic Energy Conversion, 2010, pp. 1761–1764.

[49] K.R. McIntosh, L.P. Johnson, Recombination at textured silicon surfaces passivated with silicon dioxide, J. Appl. Phys. 105 (2009) 124520, https://doi.org/10.1063/1.3153979.

[50] D.J. DiMaria, J.W. Stasiak, Trap creation in silicon dioxide produced by hot electrons, J. Appl. Phys. 65 (1989) 2342–2356, https://doi.org/10.1063/1.342824.

[51] D.A. Buchanan, A.D. Marwick, D.J. DiMaria, L. Dori, Hot-electron-induced hydrogen redistribution and defect generation in metal-oxide-semiconductor capacitors, J. Appl. Phys. 76 (1994) 3595–3608, https://doi.org/10.1063/1.357420.

[52] G. Bourret-Sicotte, P.G. Hamer, D. Tweddle, R.S. Bonilla, P.R. Wilshaw, Hydrogen related defects in float zone silicon investigated using a shielded hydrogen plasma, in: 2018 IEEE 7th World Conference on Photovoltaic Energy Conversion, WCPEC 2018 - A Joint Conference of 45th IEEE PVSC, 28th PVSEC and 34th EU PVSEC, 2018, pp. 298–302, https://doi.org/10.1109/PVSC.2018.8547713.

[53] A.C. nee Wenham, S. Wenham, R. Chen, C. Chan, D. Chen, B. Hallam, D. Payne, T. Fung, M. Kim, S. Liu, S. Wang, K. Kim, A. Samadi, C. Sen, C. Vargas, U. Varshney, B.V. Stefani, P. Hamer, G. Bourret-Sicotte, N. Nampalli, Z. Hameiri, C. Chong, M. Abbott, Hydrogen-induced degradation, in: 2018 IEEE 7th World Conference on Photovoltaic Energy Conversion (WCPEC) (A Joint Conference of 45th IEEE PVSC, 28th PVSEC & 34th EU PVSEC), IEEE, 2018, pp. 1–8, https://doi.org/10.1109/PVSC.2018.8548100.

[54] D. Chen, P.G. Hamer, M. Kim, T.H. Fung, G. Bourret-Sicotte, S. Liu, C.E. Chan, A. Ciesla, R. Chen, M.D. Abbott, B.J. Hallam, S.R. Wenham, Hydrogen induced degradation: a possible mechanism for light- and elevated temperature- induced degradation in n-type silicon, Sol. Energy Mater. Sol. Cell. 185 (2018) 174–182, https://doi.org/10.1016/J.SOLMAT.2018.05.034.

[55] B. Tuttle, Energetics and diffusion of hydrogen in SiO2, Phys. Rev. B 61 (2000) 4417–4420, https://doi.org/10.1103/PhysRevB.61.4417.

[56] W.G. Perkins, D.R. Begeal, Diffusion and permeation of He, Ne, Ar, Kr, and D2 through silicon oxide thin films, J. Chem. Phys. 54 (1971), https://doi.org/10.1063/1.1675072.

[57] R.S. Bonilla, F. Woodcock, P.R. Wilshaw, Very low surface recombination velocity in n-type c-Si using extrinsic field effect passivation, J. Appl. Phys. 116 (2014) 054102, https://doi.org/10.1063/1.4892099.

[58] R.S. Bonilla, B. Hoex, P. Hamer, P.R. Wilshaw, Dielectric surface passivation for silicon solar cells: a review, Phys. Status Solidi 214 (2017) 1700293, https://doi.org/10.1002/pssa.201700293.

[59] S.C. Baker-Finch, K.R. McIntosh, The contribution of planes, vertices, and edges to recombination at pyramidally textured surfaces, IEEE J. Photovoltaics 1 (2011) 59–65, https://doi.org/10.1109/JPHOTOV.2011.2165530.

[60] T.C. Kho, K. Fong, K. McIntosh, E. Franklin, N. Grant, M. Stocks, S.P. Phang, Y. Wan, E.C. Wang, K. Vora, Z. Ngwe, A. Blakers, Exceptional silicon surface passivation by an ONO dielectric stack, Sol. Energy Mater. Sol. Cell. 189 (2019) 245–253, https://doi.org/10.1016/j.solmat.2018.05.061.

[61] P. Masuch, C. Reichel, R.S. Bonilla, A. Richter, J. Benick, Bias-voltage photoconductance and photoluminescence for the determination of silicon-dielectric interface properties in SiO2/Al2O3 stacks, J. Appl. Phys. 134 (2023), https://doi.org/10.1063/5.0153204.

[62] C. Leguijt, P. Lölgen, J.A.A. Eikelboom, A.W.W. Weeber, F.M.M. Schuurmans, W. C.C. Sinke, P.F.A.F.A. Alkemade, P.M.M. Sarro, C.H.M.H.M. Marée, L.A. A. Verhoef, Low temperature surface passivation for silicon solar cells, Sol. Energy Mater. Sol. Cell. 40 (1996) 297–345, https://doi.org/10.1016/0927-0248(95)00155-7.

[63] R. Hezel, K. Blumenstock, R. Schörner, Interface states and fixed charges in MNOS structures with APCVD and plasma silicon nitride, J. Electrochem. Soc. 131 (1984) 1679, https://doi.org/10.1149/1.2115936.

[64] G.G. DeLeo, W.B. Fowler, G.D. Watkins, Electronic structure of hydrogen- and alkali-metal-vacancy complexes in silicon, Phys. Rev. B 29 (1984) 1819–1823, https://doi.org/10.1103/PhysRevB.29.1819.

[65] J.-U. Sachse, E.Ö. Sveinbjörnsson, N. Yarykin, J. Weber, Similarities in the electrical properties of transition metal–hydrogen complexes in silicon, Mater. Sci. Eng., B 58 (1999) 134–140, https://doi.org/10.1016/S0921-5107(98)00282-7.

[66] T. Sadoh, M. Watanabe, H. Nakashima, T. Tsurushima, Deep levels of chromium-hydrogen complexes in silicon, J. Appl. Phys. 75 (1994) 3978–3981, https://doi.org/10.1063/1.356018.

[67] R.S. Bonilla, C. Reichel, M. Hermle, P.R. Wilshaw, Extremely low surface recombination in 1 Ω cm n-type monocrystalline silicon, Phys. Status Solidi Rapid Res. Lett. 1 (2016) 1–5, https://doi.org/10.1002/pssr.201600307.

[68] Z. Xin, S. Duttagupta, M. Tang, Z. Qiu, B. Liao, A.G. Aberle, R. Stangl, An improved methodology for extracting the interface defect density of passivated silicon solar cells, IEEE J. Photovoltaics 6 (2016) 1080–1089, https://doi.org/10.1109/JPHOTOV.2016.2576685.

[69] H. Guthrey, C. Lima Salles, A.S. Kale, W. Nemeth, M. Page, S. Agarwal, D. L. Young, M. Al-Jassim, P. Stradins, Effect of surface texture on pinhole formation in SiO x-based passivated contacts for high-performance silicon solar cells, ACS Appl. Mater. Interfaces 12 (2020), https://doi.org/10.1021/acsami.0c12795.

[70] A.W. Weeber, H. Rieffe, W. Sinke, W.J. Soppe, Structural and passivating properties of SiNx:H deposited under different precursor gases, in: Proceedings of the 19th European Photovoltaic Solar Energy Conference, 2004, pp. 7–11.

[71] D. Bredemeier, D.C. Walter, R. Heller, J. Schmidt, Impact of hydrogen-rich silicon nitride material properties on light-induced lifetime degradation in multicrystalline silicon, Phys. Status Solidi Rapid Res. Lett. 13 (2019) 1900201, https://doi.org/10.1002/pssr.201900201.

[72] J.-F. Lelièvre, E. Fourmond, A. Kaminski, O. Palais, D. Ballutaud, M. Lemiti, Study of the composition of hydrogenated silicon nitride SiNx:H for efficient surface and bulk passivation of silicon, Sol. Energy Mater. Sol. Cell. 93 (2009) 1281–1289, https://doi.org/10.1016/j.solmat.2009.01.023.

[73] V. Sharma, C. Tracy, D. Schroder, S. Herasimenka, W. Dauksher, S. Bowden, Manipulation of K center charge states in silicon nitride films to achieve excellent surface passivation for silicon solar cells, Appl. Phys. Lett. 104 (2014) 053503, https://doi.org/10.1063/1.4863829.

[74] Y. Wan, K.R. McIntosh, A.F. Thomson, Characterisation and optimisation of PECVD SiNx as an antireflection coating and passivation layer for silicon solar cells, AIP Adv. 3 (2013) 032113, https://doi.org/10.1063/1.4795108.

[75] B.J. Hallam, P.G. Hamer, A.M. Ciesla née Wenham, C.E. Chan, B. Vicari Stefani, S. Wenham, Development of advanced hydrogenation processes for silicon solar cells via an improved understanding of the behaviour of hydrogen in silicon, Prog. Photovoltaics Res. Appl. 28 (2020) 1217–1238, https://doi.org/10.1002/pip.3240.

[76] P. Balk, Effects of hydrogen annealing on silicon surfaces, in: Electrochemical Society Spring Meeting, 1965, pp. 237–240.

[77] T. Mueller, S. Schwertheim, W.R. Fahrner, Application of wide-bandgap hydrogenated amorphous silicon oxide layers to heterojunction solar cells for high quality passivation, in: 2008 33rd IEEE Photovolatic Specialists Conference, IEEE, 2008, pp. 1–6, https://doi.org/10.1109/PVSC.2008.4922792.

[78] A. Stesmans, V.V. Afanas'ev, Invasive nature of corona charging on thermal Si/SiO2 structures with nanometer-thick oxides revealed by electron spin resonance, Appl. Phys. Lett. 82 (2003) 2835–2837, https://doi.org/10.1063/1.1540245.

[79] A. Stesmans, Passivation of P_b0 and P_b1 interface defects in thermal (100) Si/SiO2 with molecular hydrogen, Appl. Phys. Lett. 68 (1996) 2076–2078, https://doi.org/10.1063/1.116308.

[80] J.H. Stathis, Dissociation kinetics of hydrogen-passivated (100) Si/SiO2 interface defects, J. Appl. Phys. 77 (1995) 6205–6207, https://doi.org/10.1063/1.359148.

[81] J.M.M. de Nijs, K.G. Druijf, V.V. Afanas'ev, E. van der Drift, P. Balk, Hydrogen induced donor-type Si/SiO2 interface states, Appl. Phys. Lett. 65 (1994) 2428–2430, https://doi.org/10.1063/1.112696.

[82] K.L. Brower, Kinetics of H2 passivation of Pb centers at the (111) Si-SiO2 interface, Phys. Rev. B 38 (1988) 9657–9666, https://doi.org/10.1103/PhysRevB.38.9657.

[83] N.H. Thoan, K. Keunen, V.V. Afanas'ev, A. Stesmans, Interface state energy distribution and Pb defects at Si(110)/SiO2 interfaces: comparison to (111) and (100) silicon orientations, J. Appl. Phys. 109 (2011), https://doi.org/10.1063/1.3527909.

[84] K.L. Brower, S.M. Myers, Chemical kinetics of hydrogen and (111) Si-SiO2 interface defects, Appl. Phys. Lett. 57 (1990) 162–164, https://doi.org/10.1063/1.103971.

[85] A. Stesmans, Revision of H2 passivation of Pb interface defects in standard (111) Si/SiO2, Appl. Phys. Lett. 68 (1996) 2723–2725, https://doi.org/10.1063/1.115577.

[86] L.-Å. Ragnarsson, P. Lundgren, Electrical characterization of Pb centers in (100) Si–SiO2 structures: the influence of surface potential on passivation during post metallization anneal, J. Appl. Phys. 88 (2000) 938–942, https://doi.org/10.1063/1.373759.

[87] A. Stesmans, Comparative analysis of the H2 passivation of interface defects at the interface using electron spin resonance, Solid State Commun. 97 (1996) 255–259, https://doi.org/10.1016/0038-1098(95)00535-8.

[88] K.L. Brower, Dissociation kinetics of hydrogen-passivated (111) Si-SiO2 interface defects, Phys. Rev. B 42 (1990) 3444–3453, https://doi.org/10.1103/PhysRevB.42.3444.

[89] M.L. Reed, J.D. Plummer, Chemistry of Si-SiO2 interface trap annealing, J. Appl. Phys. 63 (1988) 5776, https://doi.org/10.1063/1.340317.

[90] A. Stesmans, V.V. Afanas'ev, Thermally induced interface degradation in (100) and (111) Si/SiO2 analyzed by electron spin resonance, J. Vac. Sci. Technol. B: Microelectron. Nanometer Struct.–Process., Meas., Phenom. 16 (1998) 3108–3111, https://doi.org/10.1116/1.590449.

[91] F.J. Feigl, D.R. Young, D.J. DiMaria, S. Lai, J. Calise, The effects of water on oxide and interface trapped charge generation in thermal SiO2 films, J. Appl. Phys. 52 (1981) 5665–5682, https://doi.org/10.1063/1.329502.

[92] L. Do Thanh, P. Balk, Elimination and generation of Si - SiO2 interface traps by low temperature hydrogen annealing, J. Electrochem. Soc. 135 (1988) 1797–1801, https://doi.org/10.1149/1.2096133.

[93] H. Jin, K.J. Weber, N.C. Dang, W.E. Jellett, Defect generation at the Si–SiO2 interface following corona charging, Appl. Phys. Lett. 90 (2007), https://doi.org/10.1063/1.2749867.

[94] Z.J. Rad, J.-P. Lehtiö, I. Mack, K. Rosta, K. Chen, V. Vähänissi, M. Punkkinen, R. Punkkinen, H.-P. Hedman, A. Pavlov, M. Kuzmin, H. Savin, P. Laukkanen, K. Kokko, Decreasing interface defect densities via silicon oxide passivation at temperatures below 450 °C, ACS Appl. Mater. Interfaces 12 (2020) 46933–46941, https://doi.org/10.1021/acsami.0c12636.

[95] Z.A. Weinberg, Hole injection and transport in SiO2 films on Si, Appl. Phys. Lett. 27 (1975), https://doi.org/10.1063/1.88522.

[96] M.H. Woods, R. Williams, Hole traps in silicon dioxide, J. Appl. Phys. 47 (1976), https://doi.org/10.1063/1.322730.

[97] Z.A. Weinberg, W.C. Johnson, M.A. Lampert, High-field transport in SiO2 on silicon induced by corona charging of the unmetallized surface, J. Appl. Phys. 47 (1976), https://doi.org/10.1063/1.322307.

[98] R.E. Stahlbush, A.H. Edwards, D.L. Griscom, B.J. Mrstik, Post-irradiation cracking of H2 and formation of interface states in irradiated metal-oxide-semiconductor field-effect transistors, J. Appl. Phys. 73 (1993), https://doi.org/10.1063/1.353348.

[99] V.V. Afanas'ev, M. Depas, J.M.M. de Nijs, P. Balk, Simultaneous elimination of electrically active defects in Si/SiO2 structures by implanted fluorine, Microelectron. Eng. 22 (1993) 93–96, https://doi.org/10.1016/0167-9317(93)90138-U.

[100] Q.D.M. Khosru, N. Yasuda, K. Taniguchi, C. Hamaguchi, Spatial distribution of trapped holes in SiO2, J. Appl. Phys. 76 (1994) 4738–4742, https://doi.org/10.1063/1.357242.
[101] J.F. Chen, Kuen-Shiuan Tian, Shiang-Yu Chen, Kuo-Ming Wu, J.R. Shih, K. Wu, An investigation on anomalous hot-carrier-induced on-resistance reduction in n-type LDMOS transistors, IEEE Trans. Device Mater. Reliab. 9 (2009) 459–464, https://doi.org/10.1109/TDMR.2009.2025770.
[102] S.W. Glunz, F. Feldmann, SiO2 surface passivation layers – a key technology for silicon solar cells, Sol. Energy Mater. Sol. Cell. 185 (2018) 260–269, https://doi.org/10.1016/j.solmat.2018.04.029.
[103] B.L. Sopori, X. Deng, J.P. Benner, A. Rohatgi, P. Sana, S.K. Estreicher, Y.K. Park, M.A. Roberson, Hydrogen in silicon: a discussion of diffusion and passivation mechanisms, Sol. Energy Mater. Sol. Cell. 41–42 (1996) 159–169, https://doi.org/10.1016/0927-0248(95)00098-4.
[104] B.R. Tuttle, W. McMahon, K. Hess, Hydrogen and hot electron defect creation at the Si(100)/SiO2interface of metal-oxide-semiconductor field effect transistors, Superlattice. Microst. 27 (2000) 229–233, https://doi.org/10.1006/spmi.1999.0804.
[105] M. Houssa, J.L. Autran, M.M. Heyns, A. Stesmans, Model for defect generation at the (1 0 0)Si/SiO2 interface during electron injection in MOS structures, Appl. Surf. Sci. 212–213 (2003) 749–752, https://doi.org/10.1016/S0169-4332(03)00042-4.
[106] V.V. Afanas'ev, A. Stesmans, Hydrogen release related to hole injection into SiO2 layers on Si, Mater. Sci. Semicond. Process. 4 (2001) 149–151, https://doi.org/10.1016/S1369-8001(00)00151-7.